Supporting Information

Lerch et al. 10.1073/pnas.1506505112

SI Materials and Methods

High-Pressure Far-UV CD. High-pressure CD was done as described in Lerch et al. (1). Briefly, the experiments were performed on a Jasco 810 spectropolarimeter at room temperature using a modified high-pressure cell. The sample concentration was 12–16 μM in buffer consisting of 10 mM MES and 25 mM NaCl at pH 6.8 for D89R1/T109R1/L99A/G113A/R119P and 5 mM MES and 2.5 mM NaCl at pH 5.5 for D89R1/T109R1/L99A. For both buffers, the baseline as a function of pressure was recorded and used for correction. The path length of the optical cell was 0.5 mm, and the scan rate used was 50 nm/min with a response time of 1 s. The sample was allowed to equilibrate for 5 min at each pressure before data collection. Each spectrum shown is an average of nine scans. Reversibility was verified by data collection after depressurization. The changes in secondary structure were quantitatively analyzed using the CONTIN algorithm (2, 3).

Model-Based Gaussian Fit of DEER Data. Fits of the background-corrected DEER dipolar evolution functions (Figs. S2, S3, and S7) to a multiple-Gaussian model for the distance distribution were performed using the software LongDistances, written in LabVIEW and available for download at http://www.chemistry.ucla.edu/directory/hubbell-wayne-l. Initial estimates for each Gaussian mean were obtained by extracting the most probable distances for each peak observed in the model-free fit with the lowest χ^2 value. During the first iteration of the fitting process for atmospheric pressure data, the mean for each Gaussian was fixed and the amplitudes and widths were allowed to vary. During subsequent iterations, the mean of each Gaussian was allowed to vary up to 0.5 Å to improve the fit. In a few cases, the lowest χ^2 value from Gaussian-based fit to the time domain data were obtained after further optimization of the baseline correction. The width of the Gaussians was in the range of 1.03–5.30 Å. For fitting of the high-pressure data, the mean and width of each Gaussian obtained at atmospheric pressure were kept constant and only the relative amplitudes were allowed to vary.

1. Lerch MT, Horwitz J, McCoy J, Hubbell WL (2013) Circular dichroism and site-directed spin labeling reveal structural and dynamical features of high-pressure states of myoglobin. *Proc Natl Acad Sci USA* 110(49):E4714–E4722.
2. Fasman GD, ed (1996) *Circular Dichroism and the Conformational Analysis of Biomolecules* (Springer, New York).
3. Sreerama N, Woody RW (2000) Estimation of protein secondary structure from circular dichroism spectra: Comparison of CONTIN, SELCON, and CDSSTR methods with an expanded reference set. *Anal Biochem* 287(2):252–260.

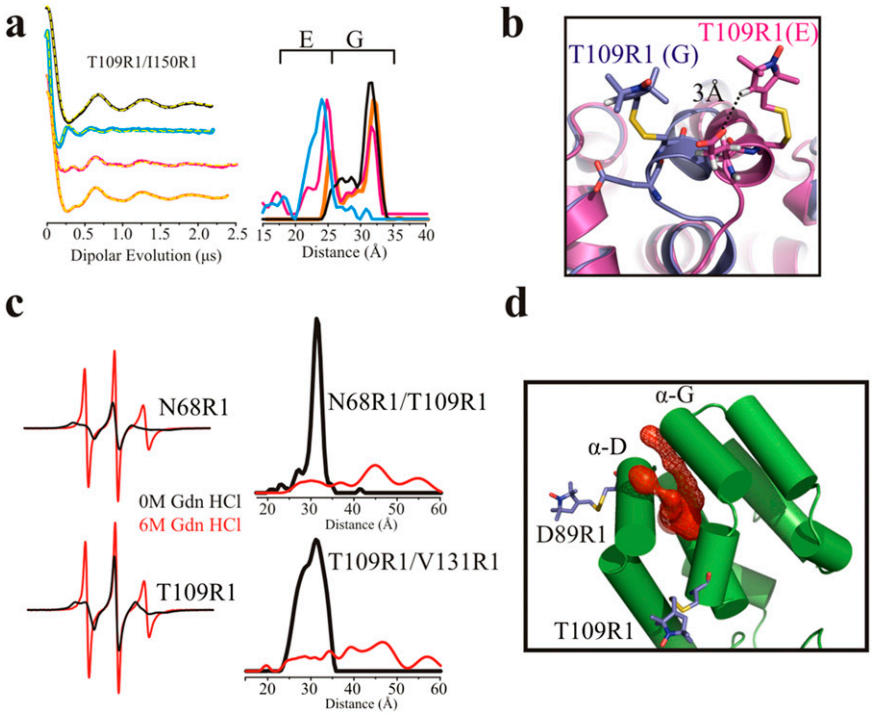

Fig. S1. SDSL-EPR data on the **G** ↔ **E** equilibrium in L99A mutants, fully unfolded forms, models of T109R1and putative tunnels in T4L L99A that could allow ligand access. (*A*) DEFs and corresponding distance distributions for T109R1/I150R1 in the WT* (black), L99A/G113A/R119P (blue), L99A/G113A (magenta), and L99A/G113A with benzene (orange). The data show that the shift to the **E** conformation is smaller in L99A/G113A compared with L99A/G113A/R119P. (*B*) Model of T109R1 in the **G** and **E** states showing possible nonclassical H-bonding interaction of the 4-H in the R1 nitroxide ring with E108 in the **E** conformation; the distance of the 4-H to E108 is too long for interaction in the **G** conformation. (*C*) Examples of CW EPR spectra (*Left*) and DEER distance distributions (*Right*) for fully folded (black) and unfolded T4L WT* in 6 M GdnHCl (red). (*D*) Ribbon diagram of T4L L99A structure showing two putative tunnels to the cavity identified by Caver analysis (1, 2) in the interface between helices D and G. The tunnels are shown in red surface representation.

1. Kozlikova B, et al. (2014) CAVER Analyst 1.0: Graphic tool for interactive visualization and analysis of tunnels and channels in protein structures. *Bioinformatics* 30(18):2684–2685.
2. Chovancova E, et al. (2012) CAVER 3.0: A tool for the analysis of transport pathways in dynamic protein structures. *PLOS Comput Biol* 8(10):e1002708.

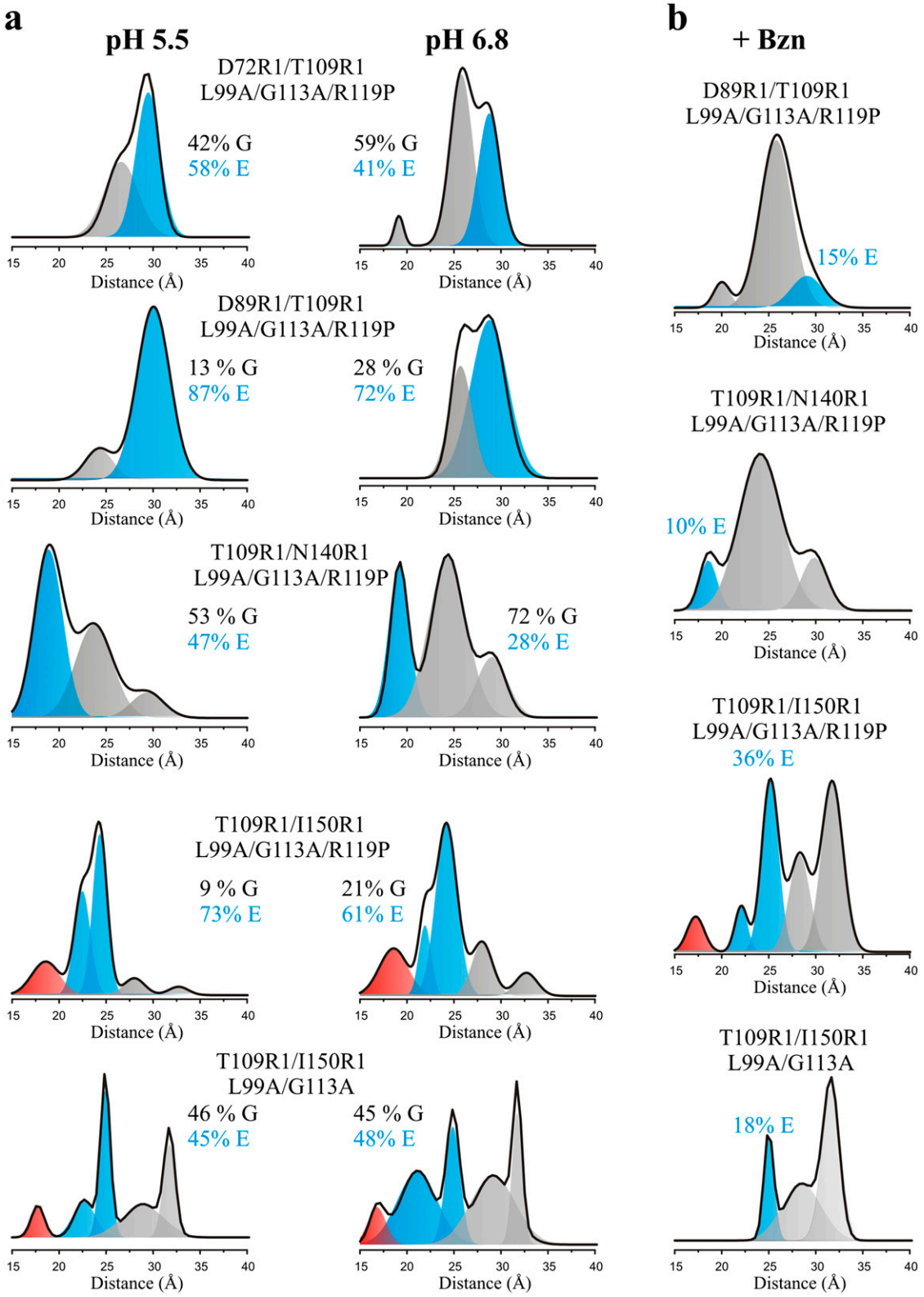

Fig. S2. Multiple Gaussian distance distributions of the indicated mutants. (*A*) Distance distributions of the indicated mutants at pH values of 5.5 and 6.8. (*B*) Distance distributions in the presence of benzene at pH 6.8. The black line is the overall distance distribution based on Gaussian fits. The Gaussians representing distances of **G** and **E** and a third state are shown in gray, blue, and red, respectively.

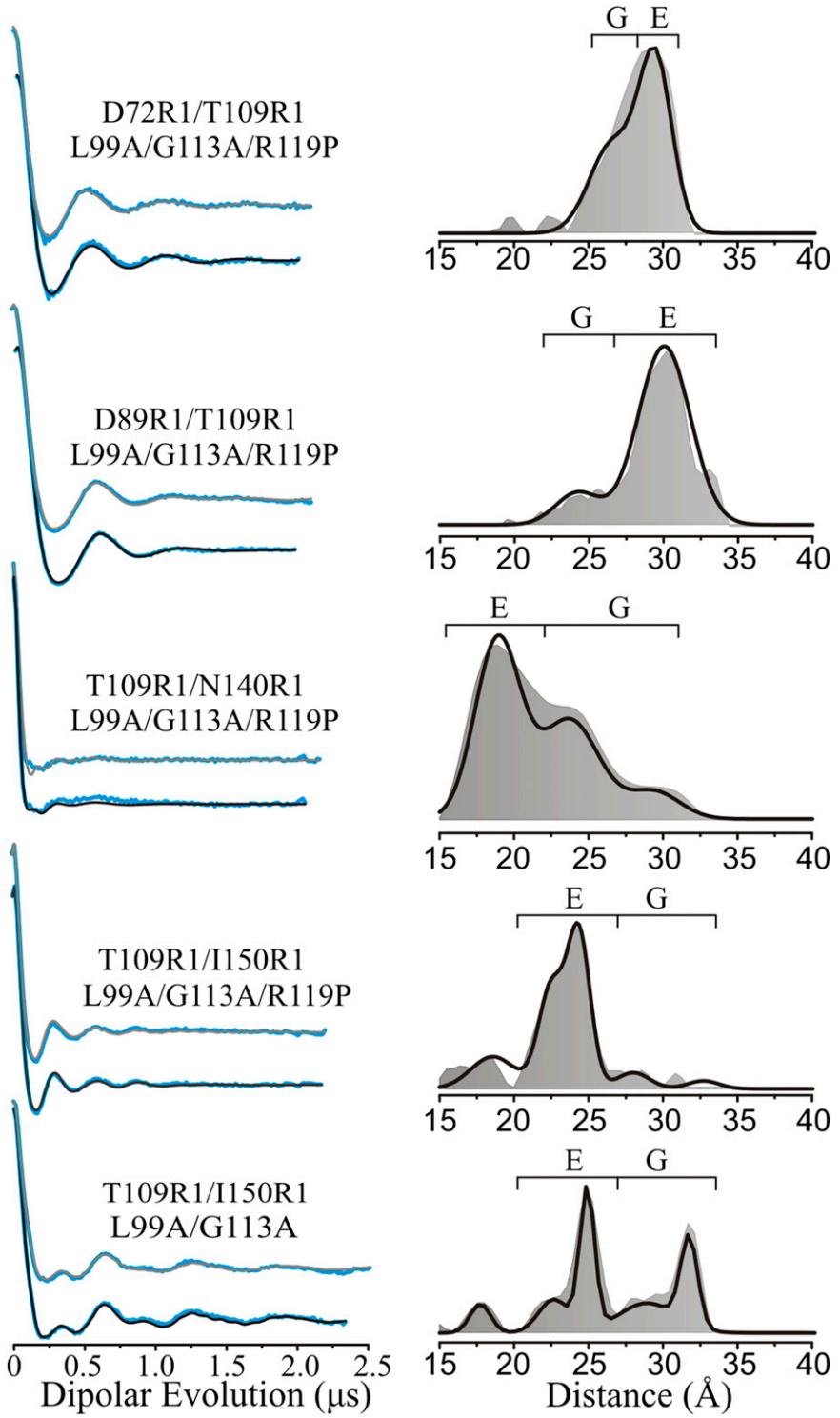

Fig. S3. Comparison of model-free and multiple Gaussian-based fits in the indicated mutants. (*Left*) Model-free fits (gray) and Gaussian-based fits (black) to the DEFs (blue) of the indicated mutants. (*Right*) Corresponding distance distributions based on model-free fit (shaded) and Gaussian-based fit (black trace) of the indicated mutants.

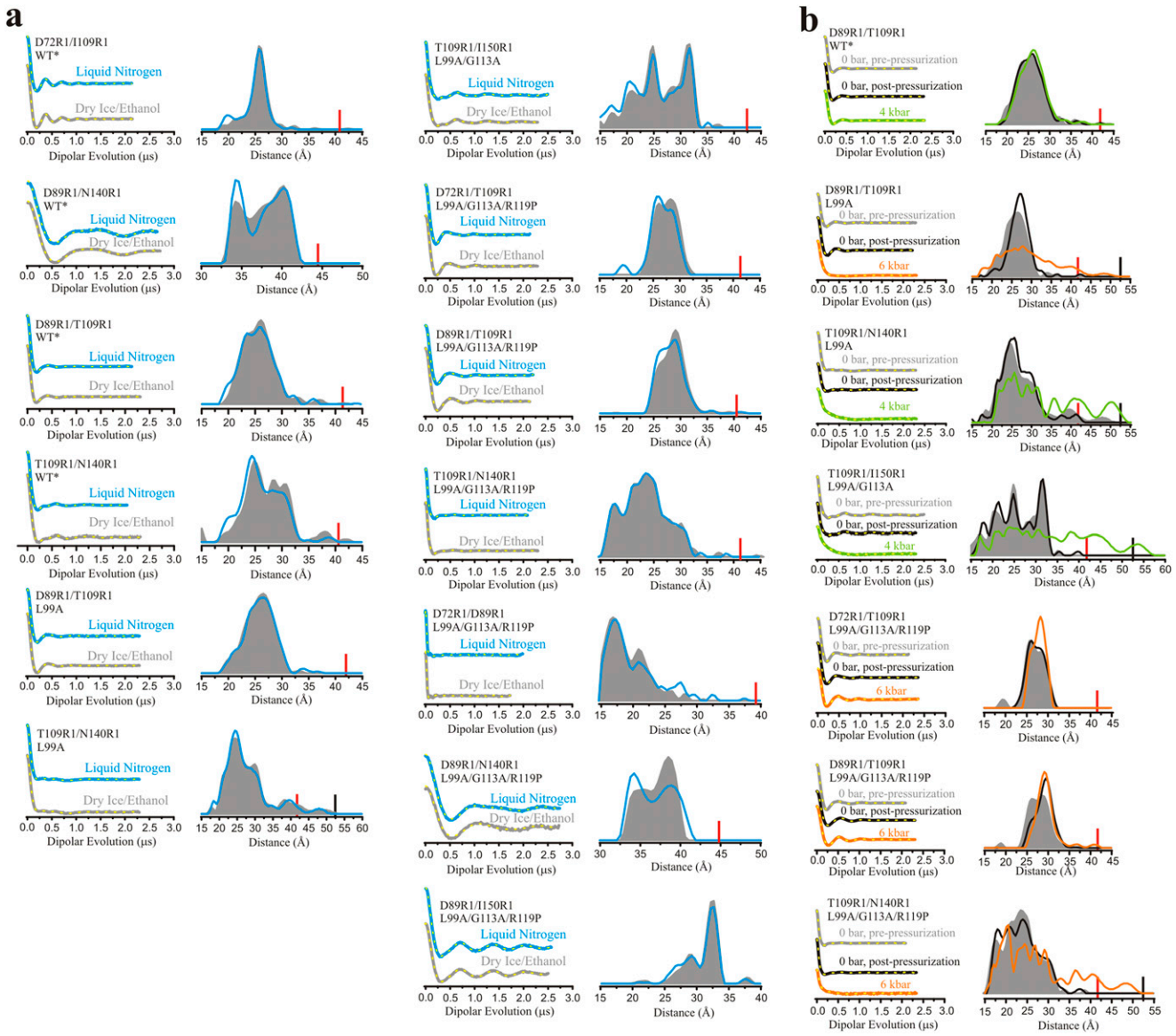

Fig. S4. Comparison of dry ice/ethanol and liquid nitrogen freezing and reversibility of changes observed with PR DEER. DEFs, model-free fits of the DEFs (dashed yellow traces), and corresponding distance distributions are shown for the indicated mutants (*A*) prepared using dry ice/ethanol and liquid nitrogen at atmospheric pressure or (*B*) at 0 bar pre- and postpressurization (data for each mutant at either 4 or 6 kbar is shown for comparison). Excellent reversibility is observed for all mutants except D89R1/T109R1 in the L99A and L99A/G113A/R119P backgrounds, which are only partially reversible after pressurization to 6 kbar. The DEFs and distance distributions are color-coded as indicated. The red and black bars indicate the upper limit of reliable shape and distance of the distribution, respectively (*Materials and Methods*).

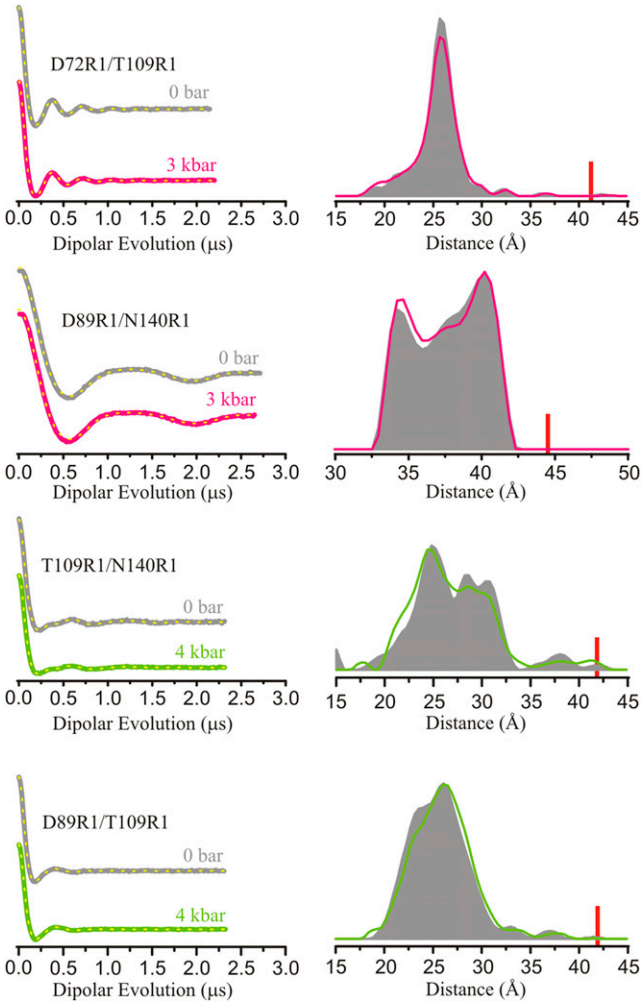

Fig. S5. PR DEER in the WT* background. DEFs, model-free fits of the DEFs (dashed yellow traces), and corresponding distance distributions are shown for the indicated doubles in the WT* background. The DEFs and distance distributions are color-coded as indicated. The red bar indicates the upper limit of reliable shape of the distribution (*Materials and Methods*).

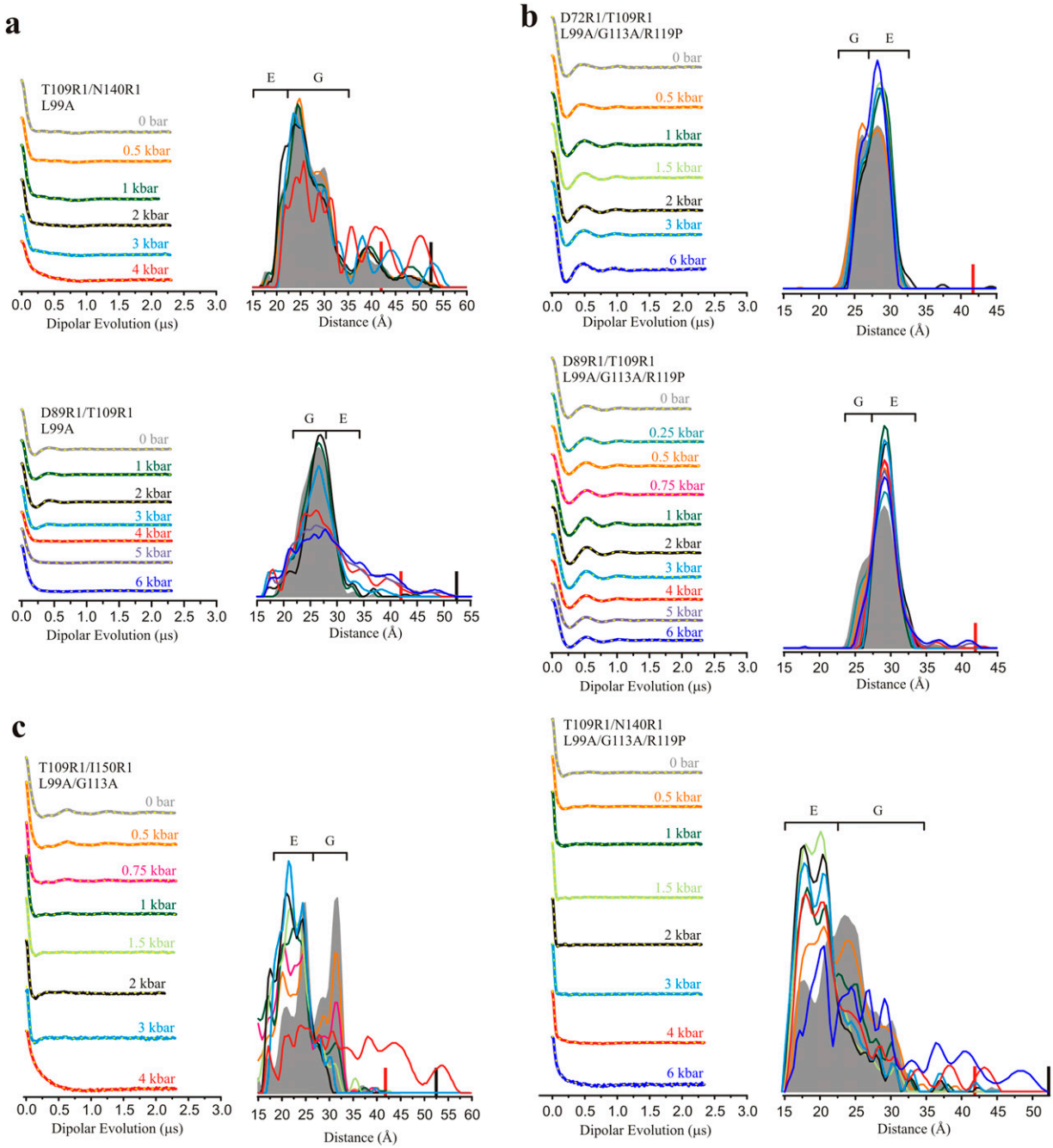

Fig. S6. PR DEER in the (*A*) L99A, (*B*) L99A/G113A/R119P, and (*C*) L99A/G113A backgrounds. DEFs, model-free fits of the DEFs (dashed yellow traces), and corresponding distance distributions are shown for the indicated doubles. The DEFs and distance distributions are color-coded as indicated. The red and black bars indicate the upper limit of reliable shape and distance of the distribution, respectively (*Materials and Methods*).

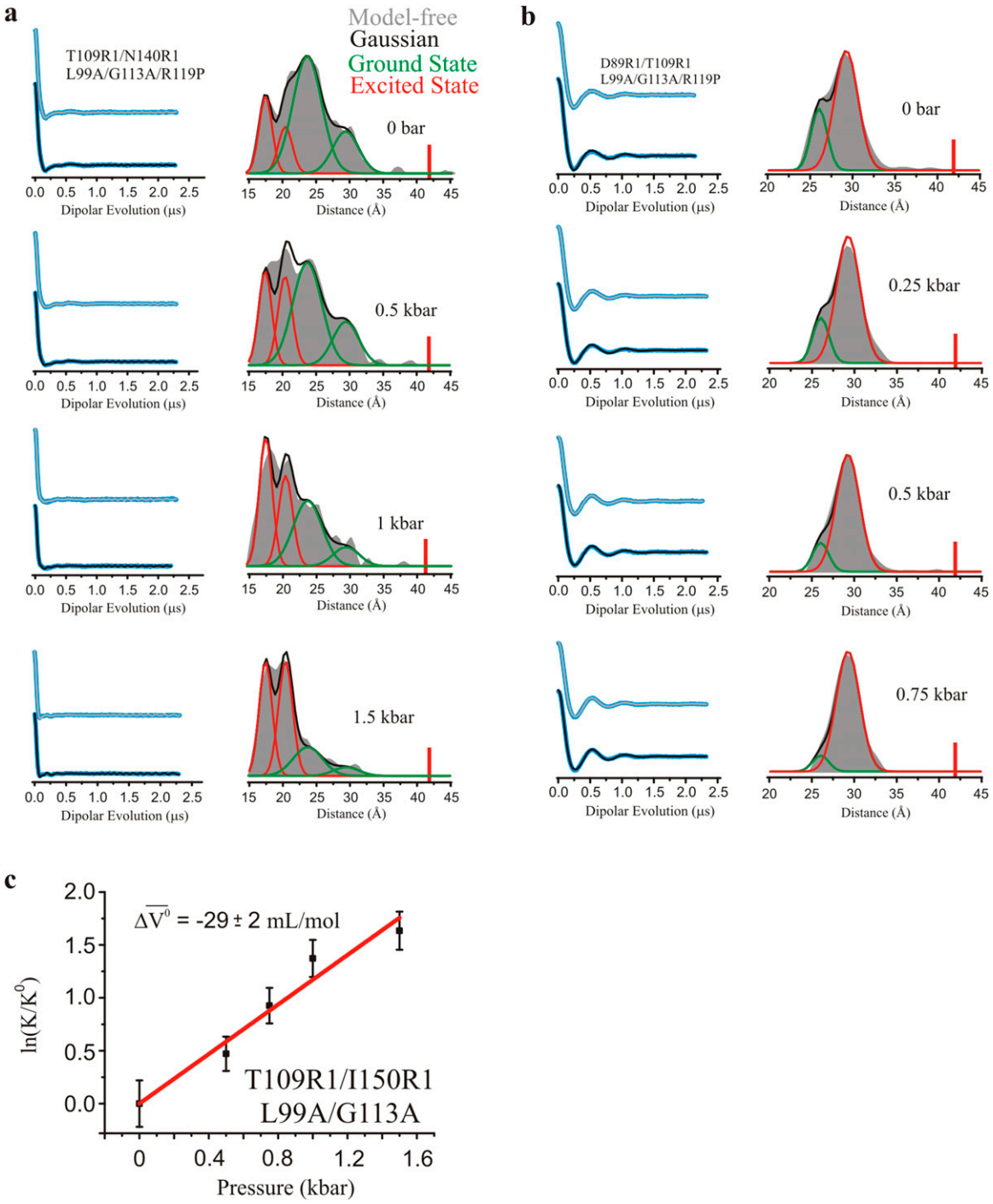

Fig. S7. Comparison of model-free and multiple Gaussian-based fits of the DEF from PR DEER. Model-free fits (gray) and Gaussian-based fits (black) to the DEF (blue) of (*A*) T109R1/N140R1/L99A/G113A/R119P and (*B*) D89R1/T109R1/L99A/G113A/R119P are shown for the indicated pressures. Corresponding distance distributions are overlaid to the right of the DEF and are color-coded according to the inset. The red bar indicates the upper limit of reliable shape of the distribution (*Materials and Methods*). (*C*) Plot of ln(K/K^{o}) vs. pressure for the indicated mutant and fit (red trace) using a two-state model to measure ΔV^{o} for the **G** → **E** transition.

Table S1. Expected and experimentally observed changes in distances from residue T109R1 to the indicated reference in the G → E transition

Mutant	$\Delta r_{G\rightarrow E}$ modeling,[†] Å	$\Delta r_{G\rightarrow E}$ experimental, Å
D72R1/T109R1	+5.0	+3.5
D89R1/T109R1	+7.0	+6.5
T109R1/N140R1	−7.5	−6.8
T109R1/I150R1	−5.0	−7.0

The expected changes in distances are based on modeling the R1 side chain in G and E (Fig. 1*A*).

[†]The R1 side chains at sites 72, 89, 109, and 140 were modeled using one of the most commonly observed R1 rotamers on X-ray structures of R1 in T4L that most closely match the experimentally determined distances. For site 150, the R1 rotamer modeled was that observed in the X-ray structure of I150R1 (1).

1. Fleissner MR (2007) *X-ray Structures of Nitroxide Side Chains in Proteins: A Basis for Interpreting Distance Measurements and Dynamic Studies by Electron Paramagnetic Resonance*. PhD thesis (Univ. of California, Los Angeles).

Table S2. Secondary structure of indicated T4L mutants as a function of pressure determined from CD

Mutant	Pressure, kbar	α-Helix[†]	β-Sheet	Turn	Unordered
D89R1/T109R1/L99A	0	0.58	0.09	0.14	0.19
	2.4	0.59	0.08	0.14	0.19
D89R1/T109R1/ L99A/G113A/R119P	0	0.57	0.06	0.14	0.23
	2.4	0.59	0.05	0.15	0.21
L99A[‡]	N/A	0.62	0.07		
L99A/G113A/ 119P[§]	N/A	0.59	0.07		

N/A, not applicable.

[†]Fraction of secondary structure at each pressure was estimated using the CONTIN algorithm (1, 2).

[‡],[§]Values for α-helix and β-sheets obtained from structures deposited in Protein Data Bank (PDB ID codes 1L90 and 2LC9).

1. Fasman GD, ed (1996) *Circular Dichroism and the Conformational Analysis of Biomolecules* (Springer, New York).
2. Sreerama N, Woody RW (2000) Estimation of protein secondary structure from circular dichroism spectra: Comparison of CONTIN, SELCON, and CDSSTR methods with an expanded reference set. *Anal Biochem* 287(2):252–260.